Received: 6 March 2024 | Revised: 13 April 2024 | Accepted: 6 May 2024

DOI: 10.1002/jnm.3248

RESEARCH ARTICLE

WILEY

Miniaturized IPD band pass filter with low insertion loss based on modified T-section for 5G applications

Qi Zhang | Yazi Cao | Gaofeng Wang

Ministry of Education and Engineering Research Center of Smart Microsensors and Microsystems, School of Electronics and Information, Hangzhou Dianzi University, Hangzhou, China

Correspondence
Yazi Cao, Ministry of Education and Engineering Research Center of Smart Microsensors and Microsystems, School of Electronics and Information, Hangzhou Dianzi University, Hangzhou, China.
Email: caoyazi@hdu.edu.cn

Funding information
Zhejiang Provincial Key Research & Development Project, Grant/Award Number: 2021C01041; National Natural Science Foundation of China, Grant/Award Numbers: 92373202, 62141409; National Key Research and Development Program of China, Grant/Award Number: 2019YFB2205003

Abstract

A miniaturized bandpass filter (BPF) with low insertion loss based on a modified T-section and a grounded transmission-zero resonator is proposed. The novel T-section consists of two resonators, which can achieve the bandpass performance with two transmission zeros (TZs) in the upper band. The grounded transmission-zero resonator can generate an extra transmission zero in the lower band. Therefore, high frequency selectivity can be achieved by the above three transmission zeros near the passband. The proposed BPF can achieve an insertion loss of 0.8 dB and a return loss of 22 dB covering 3.3–4.2 GHz, and the upper-stopband attenuation is better than 20 dB up to 12.5 GHz ($3.3f_0$). The proposed BPF with a miniaturized size of 1.2 mm × 0.5 mm × 0.3 mm have been fabricated using Si-based integrated passive devices (IPDs) technology and measured by on-wafer probing. The simulated and measured results of the proposed BPF are in reasonably good agreement.

KEYWORDS

bandpass filter (BPF), low insertion loss, transmission zero, T-section

1 | INTRODUCTION

Miniaturized bandpass filters (BPFs) with low insertion loss, which can significantly reduce the size and meet the requirements of high integration and miniaturization of RF front-end circuits,[1–4] have been one of critical components in 5G communication systems. Among the studies reported, there are various designs to achieve low loss, such as BPF with stacked double-layer structure,[1] low-loss filter based on folded planar waveguide,[5] self-packaged BPF,[3] BPF based on multilayer groove gap waveguide,[6] BPF based on LTCC technology,[7,8] surface acoustic wave BPF[9] and BPF based on integrated passive device (IPD) technology,[2,10] and so on.

Although the designs above have achieved low insertion loss, the chip sizes are usually too large to be integrated into RF front-end circuits. Like the BPF based on the waveguide,[5,6] low insertion loss can be achieved through large size in low frequency band, or miniaturization can be achieved in millimeter wave band. For LTCC technology,[7,8] because the low cost needs to be achieved through multiple layers, the size of the chip is also a thorny issue. Some BPF with novel technologies use yttrium iron garnet/gadolinium gallium garnet (YIG/GGG) film structures to achieve low-loss[11] but their insertion loss is still unable to meet the requirements for 5G communication. To reduce size, BPFs based on IPD technology have been proposed. A BPF design with multiple transmission zeros, which can achieve an insertion loss of 1.28 dB, was reported.[2] In addition, an E-shaped dual-mode resonator and stepped impedance resonators were adopted in a BPF design to achieve an insertion loss of 1.2 dB.[10] These two designs can reduce the chip size, but the insertion loss is still high.

In this work, a BPF with an insertion loss less than 0.8 dB and a miniaturized size of 1.2 mm × 0.5 mm × 0.3 mm is proposed. A modified T-section that generates two transmission zeros in the upper band is adopted in the proposed BPF. A grounded transmission-zero resonator is added to generate an extra transmission zero in the lower band. With these three transmission zeros, the frequency selectivity of the proposed BPF can be significantly improved. Section 2 discusses the operating principle of the modified topology, followed by the simulation and measurement results in Section 3. Finally, some conclusion is drawn in Section 4.

2 | PROPOSED BAND-PASS FILTER DESIGN

The modified T-section topology is shown in Figure 1A. It is composed of two transmission-zero resonators and a capacitor (C_5) grounded. As shown in Figure 1B, the modified T-section can achieve a bandpass performance with two transmission zeros in upper band. And the two transmission-zero resonators can be controlled by adjusting the values of the capacitors and inductors in the modified T-section. To demonstrate the mechanism of the transmission zeros generated by the modified T-section, the ABCD matrix of its two ports network can be obtained as,

$$\begin{aligned}\begin{pmatrix} A & B \\ C & D \end{pmatrix} &= \begin{pmatrix} 1 & Z_1 \\ 0 & 1 \end{pmatrix}\begin{pmatrix} 1 & 0 \\ Y & 1 \end{pmatrix}\begin{pmatrix} 1 & Z_2 \\ 0 & 1 \end{pmatrix} \\ &= \begin{pmatrix} 1+YZ_1 & Z_2+YZ_1Z_2+Z_1 \\ Y & YZ_2+1 \end{pmatrix},\end{aligned} \tag{1}$$

with

$$Z_1 = \frac{1-\omega^2 L_1 C_2}{j\omega[(C_1+C_2)-\omega^2 C_1 L_1 C_2]},$$

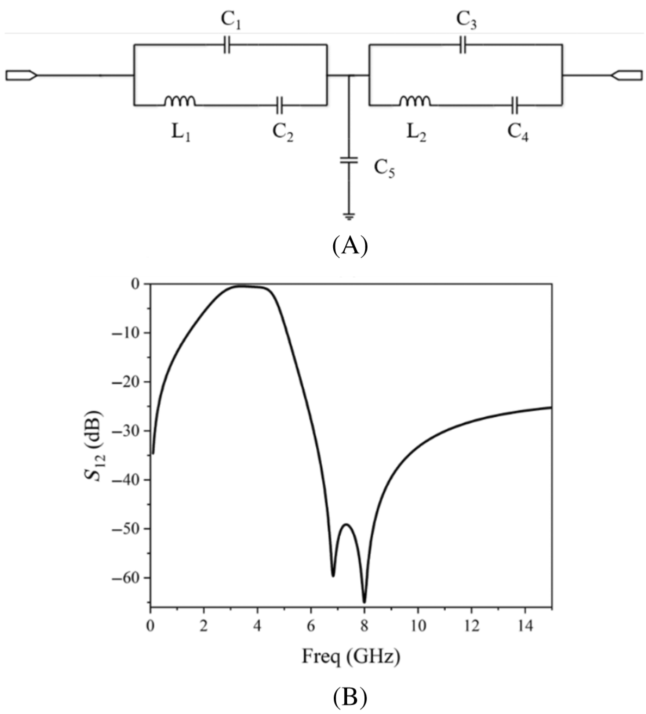

FIGURE 1 Topology and S_{12} of the modified T-section. (A) Topology and (B) S_{12}.

$$Y = j\omega C_5,$$

$$Z_2 = \frac{1-\omega^2 L_2 C_4}{j\omega[(C_3+C_4)-\omega^2 C_3 L_2 C_4]},$$

where ω is the transmission frequency of the filter. The S parameters to ABCD matrix are given as follow:

$$S_{12} = \frac{2(AD-BC)}{A+B/Z_0+CZ_0+D}, \tag{2}$$

$$S_{21} = \frac{2}{A+B/Z_0+CZ_0+D}. \tag{3}$$

When $S_{12}=0$, the values of ω can be determined as,

$$\begin{cases} \omega_1 = 0 \\ \omega_2 = \sqrt{\dfrac{C_1+C_2}{L_1C_1C_2}}, \\ \omega_3 = \sqrt{\dfrac{C_3+C_4}{L_2C_3C_4}} \end{cases} \tag{4}$$

where $C_1 = 2.1$ pF, $C_2 = 1.21$ pF, $L_1 = 5.8$ nH, $C_3 = 0.58$ pF, $C_4 = 1.5$ pF, and $L_2 = 1.3$ nH in the modified T-section. The three transmission zeros are achieved in DC, 6.8 and 8.0 GHz. And according to the Equation (4), as the value of the capacitors and inductors vary, the position of the two transmission zeros can be adjusted. Therefore, the two transmission zeros can be designed in different frequency points.

According to the above analysis, the first resonator including L_1 can generate the transmission zero of the low frequency, while the second resonator including L_2 mainly generates the transmission zero of the high frequency, and thus the values of L_1 and L_2 can affect the positions of the two transmission zeros respectively. Figure 2 depicts the simulated S_{12} of the different values of L_1 and L_2. As shown in Figure 2, two transmission zeros have relatively large frequency-shifting effects due to different values of L_1 and L_2. When the value of L_1 increases, the low-frequency transmission zero moves to a lower frequency, and when the value of L_1 decreases, the low-frequency transmission zero moves to a higher frequency. Similarly, the value of L_2 has the same effect on the high-frequency transmission zero. When the value of L_1 increases and the value of L_2 decreases to some certain values, the two transmission zeros can coincide. Therefore, one

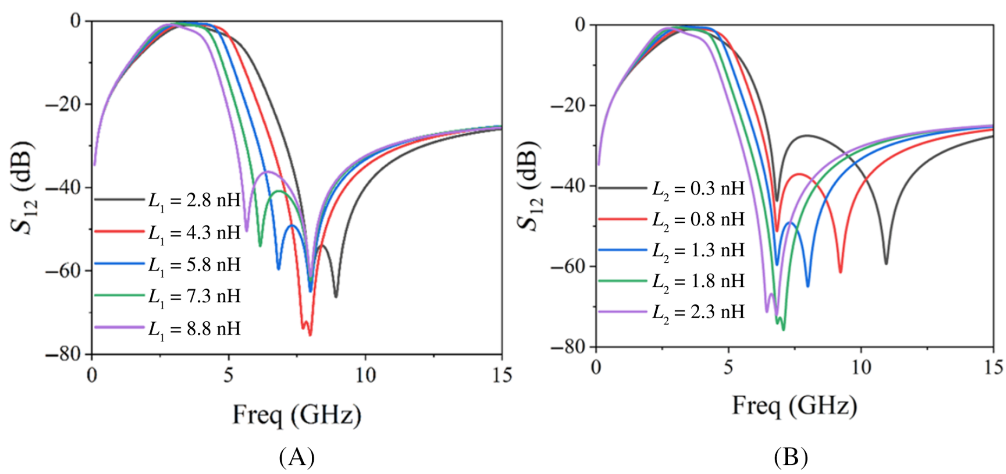

FIGURE 2 Simulated insertion loss of the proposed T-section with variations of inductor values. (A) L_1 and (B) L_2.

can adjust the two transmission zeros by adjusting the values of L_1 and L_2, so that the modified T-section can operate in different frequency bands.

The proposed BPF topology based on the above modified T-section and a grounded transmission-zero resonator is shown in Figure 3A. This grounded transmission-zero resonator is introduced to generate an extra transmission zero in the lower band. The ABCD matrix of the BPF two-port network can be given as follows:

$$\begin{pmatrix} A & B \\ C & D \end{pmatrix} = \begin{pmatrix} 1 & 0 \\ Y_1 & 1 \end{pmatrix} \begin{pmatrix} 1 & Z_1 \\ 0 & 1 \end{pmatrix} \begin{pmatrix} 1 & 0 \\ Y & 1 \end{pmatrix} \begin{pmatrix} 1 & Z_2 \\ 0 & 1 \end{pmatrix} = \begin{pmatrix} 1+Z_1Y & Z_2+Z_1Z_2Y+Z_1 \\ Y_1+Y_1YZ_1+Y & Y_1Z_2+Y_1YZ_1Z_2+YZ_2+Y_1Z_1+1 \end{pmatrix}, \tag{5}$$

where Z_1, Y, and Z_2 are the same quantities used in Equation (1), and

$$Y_1 = \frac{j\omega C_6}{1-\omega^2 L_3 C_6}.$$

According to the Equations (2) and (5), the values of ω can be determined as,

$$\omega = \frac{1}{\sqrt{L_3 C_6}}, \tag{6}$$

where $C_6 = 0.49$ pF and $L_3 = 0.82$ nH. The low-band transmission zero is located at 2.4 GHz. The S parameter S_{12} of the proposed BPF is shown in Figure 3B. From Figure 3B, this proposed topology can generate three zeros near the passband including one outside the low band and two outside the high band.

Therefore, the proposed filter is composed of the modified T-section and a grounded transmission-zero resonator. And by controlling the modified T-section and the grounded transmission-zero resonator, the proposed filter can be scaled in different frequencies.

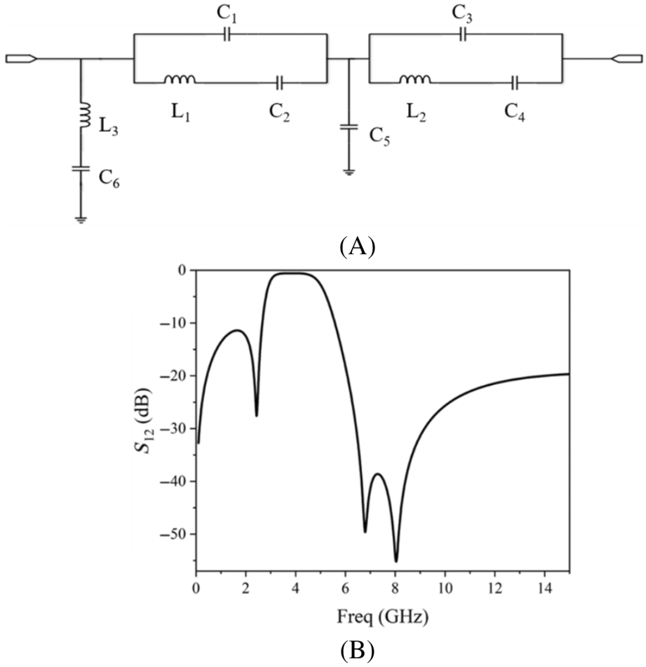

FIGURE 3 Topology and S_{12} of the proposed bandpass filter. (A) Topology and (B) S_{12}.

3 | FABRICATION AND MEASUREMENT

The proposed BPF is fabricated using the Si-based IPD technology. As shown in Figure 4, the IPD technology mainly is composed of Si substrate, oxide layer, nitride layer, and metal layers. In the Si substrate, the relative dielectric constant ε_r is 11.69, the loss tangent tanδ is 0.003, and the thickness is 250 μm. The oxide layer has a thickness of 0.1 μm, a relative dielectric constant ε_r of 3.9, and a loss tangent tanδ of 0.01. The three metal layers (M1, M2, and M3) are Cu with a thickness of 2, 6, and 8 μm, respectively. And the metal M1, M2, and M3 are connected through the metal vias. The inductors are in the M3 layer, while the MIM capacitors are in the M1 and M2 layers. Besides, the dielectric layer between capacitor is a 0.2 um thickness of SiN_X with a dielectric constant of 7.46.

The proposed BPF is simulated and its graphic design system (GDS) layout is generated by the full-wave electromagnetic simulator, UltraEM, from Faraday Dynamics, Inc.[12] Due to the influence of the parasitic parameters, the electromagnetic simulation results reveal an extra transmission zero outside the upper band than the circuit level simulation results. The fabricated BPF is measured on-chip using the Keysight N5244A PNA-X vector network analyzer and cascade summit-11000 probe station. We applied the SOLT de-embedding method during the measurement process, which is based on a 12-item error model and can reduce the impact of system errors on the measurement results, and we set the frequency step size very small during the process of measurement. Therefore, the measured curves are smooth. However, compared with the simulated results, the measured results have a slight frequency shifted in the upper band due to the fabrication tolerance. The micrograph of the proposed Si-based BPF is shown in Figure 5A, the simulated and measurement results of the proposed BPF are compared in Figure 5B. The final BPF occupies a size of 1.2×0.5 mm^2. The measured results show that the insertion loss is less than 0.8 dB, the return loss is better than 22 dB, and the upper-stopband attenuation is better than 20 dB up to 12.5 GHz ($3.3f_0$), which is in good agreement with the simulated results.

The performances of the proposal BPF and several reported BPF with low cost are compared in Table 1. Compared with the BPF fabricated on the glass substrate,[1] the proposed BPF has the same transmission zeros and insertion loss yet achieves the smaller size. Moreover, the proposed BPF can achieve lower insertion loss and smaller size in comparison with the BPF based on GaAs substrate.[2] By comparison to the BPF based on SIW[5] and LTCC,[7] the proposed BPF occupies a smaller area. Although the BPF based on the YIG/GGG from[11] can realize the miniature size, there is only one transmission zero out of the passband that cannot meet the high frequency selectivity. Compared with the design based on the same fabrication technology,[13] the proposed design can achieve the low insertion loss. Besides, the used high resistance silicon process is a mature semiconductor thin film process with good stability in processing and production. Compared with the thick film LTCC designs the yield of the final product can be greatly improved. The cost of the proposed filter is much lower than that of the GaAs process. In contrast, the proposed BPF has four transmission zeros near the passband, which can significantly improve the frequency selectivity. At the same time, due to the different actual operating frequencies and bandwidths of filters in the 5G frequency bands, we can control the operating frequency and bandwidth of this filter by adjusting the electrical dimensions of the inductance and capacitance in the in modified T-section. Therefore, the proposed filter is more suitable for the 5G applications.

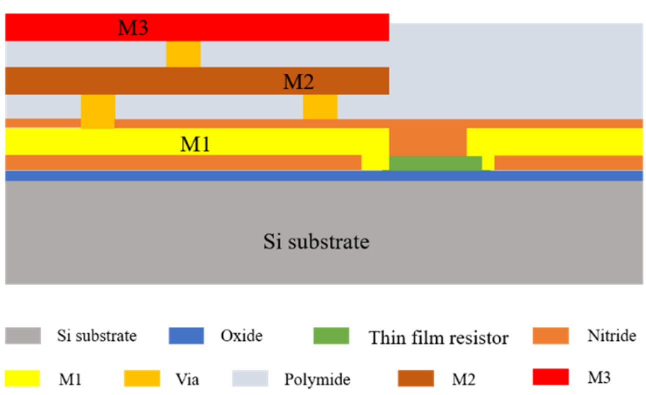

FIGURE 4 Si-based integrated passive device layer stack-up.

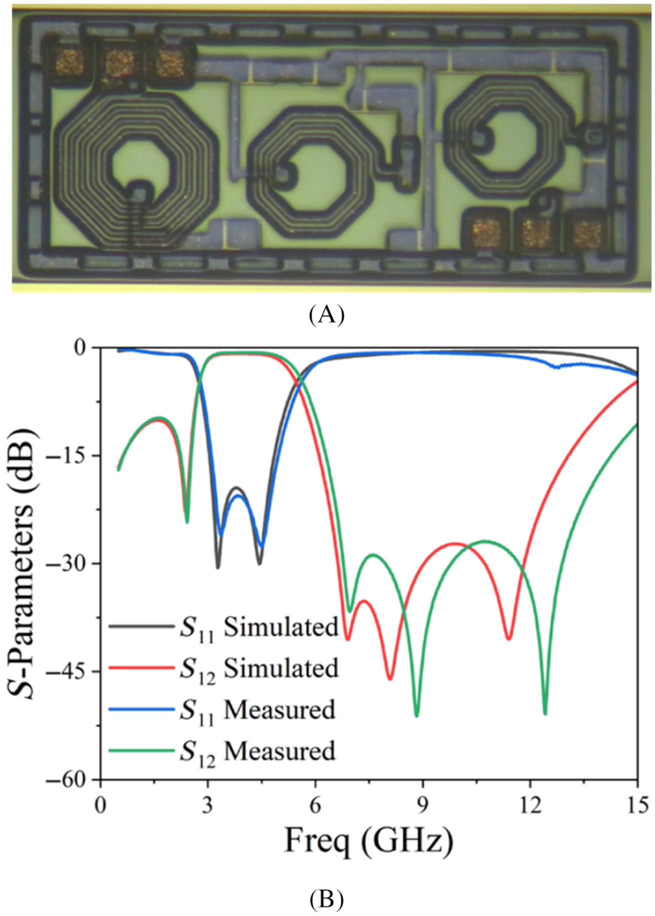

FIGURE 5 (A) Micrograph of the proposed bandpass filter (BPF) and (B) EM simulated and measured results of the proposed BPF.

TABLE 1 Comparison of the proposed bandpass filter (BPF) with several reported BPF.

Ref.	f_0 (GHz)	Insertion loss (dB)	Effective area (λ_0^2)	TZs	Tech.
1	3	0.81	0.018 × 0.013	3	Glass
2	1.93	1.17	0.254 × 0.131	7	GaAs
5	6.08	0.56	0.132 × 0.072	4	SIW
7	3.1	1.9	0.088 × 0.069	4	LTCC
11	0.0845	2	0.00197 × 0.0028	1	YIG/GGG
13	3.75	1.5	0.013 × 0.009	5	Si-based
This work	3.75	0.8	0.015 × 0.00625	4	Si-based

4 | CONCLUSIONS

In this work, a miniaturized BPF based on a modified T-section and a grounded transmission-zero resonator has been presented by virtue of the Si-based IPD technology. The modified T-section consists of two transmission-zero resonators, which can meet the bandpass performance and generate two transmission zeros out of the upper band. In addition, a grounded transmission-zero resonator has been introduced to generate a transmission zero in the lower band. The proposed BPF achieves a low insertion loss less than 0.8 dB and a wide upper stopband. The proposed BPF occupies only $1.2 \times 0.5\ \text{mm}^2$, which is a significant size reduction in comparison to previously reported BPF designs. The measurement results show a good agreement with the simulated results. The proposed BPF has a good potential in 5G communication systems.

ACKNOWLEDGMENTS

This work was supported by National Natural Science Foundation of China under grant 92373202 and 62141409, National Key Research and Development Program of China under grant 2019YFB2205003, and Zhejiang Provincial Key Research & Development Project under grant 2021C01041.

DATA AVAILABILITY STATEMENT

Data sharing is not applicable to this article as no new data were created or analyzed in this study.

ORCID

Yazi Cao https://orcid.org/0000-0001-6636-3662

REFERENCES

1. Ma H, Hu Z, Yu D. A low-loss bandpass filter with stacked double-layer structure using glass-based integrated passive device technology. *IEEE Electron Device Lett*. 2023;44(7):1216-1219.
2. Dong J, Zhu X, Yang T, Nie Y, Wang Y. On-chip wideband bandpass filter with high frequency selectivity and low insertion loss based on GaAs integrated passive device technology. Paper presented at: 2023 IEEE MTT-S International Wireless Symposium (IWS); May 14-17, 2023; Qingdao, China.
3. Chu Y, Ma K, Wang Y, Meng F. A self-packaged low-loss and compact SISL DBBPF with multiple TZs. *IEEE Microw Wirel Compon Lett*. 2019;29(3):192-194.
4. Shen G, Che W, Feng W, Shi Y, Shen Y. Low insertion-loss MMIC bandpass filter using lumped-distributed parameters for 5G millimeter-wave application. *IEEE Trans Compon Packag Manuf Technol*. 2021;11(1):98-108.
5. Tian H, Dong Y. Wideband low-loss filter with compact size and wide stopband based on folded planar waveguide. *IEEE Microw Wirel Technol Lett*. 2023;33(6):651-654.
6. Xiu T, Yao Y, Jiang H, et al. Design of a compact and low-loss E-band filter based on multilayer groove gap waveguide. *IEEE Microw Wirel Compon Lett*. 2021;31(11):1211-1214.
7. Feng W, Gao X, Che W, Yang W, Xue Q. LTCC wideband bandpass filters with high performance using coupled lines with open/shorted stubs. *IEEE Trans Compon Packag Manuf Technol*. 2017;7(4):602-609.
8. Shen G, Che W, Feng W, Shi Y, Xu F, Xue Q. Ultra-low-loss millimeter-wave LTCC bandpass filters based on flexible design of lumped and distributed circuits. *IEEE Trans Circuits Syst II Express Briefs*. 2021;68(4):1123-1127.
9. Su R, Shen J, Lu Z, et al. Wideband and low-loss surface acoustic wave filter based on 15° YX-$LiNbO_3$/SiO_2/Si structure. *IEEE Electron Device Lett*. 2021;42(3):438-441.
10. Li L-P, Shen W, Ding J-Y, Sun X-W. Compact 60-GHz on-chip bandpass filter with low insertion loss. *IEEE Electron Device Lett*. 2018;39(1):12-14.
11. Du S, Yang Q, Fan X, Wang M, Zhang H. A compact and low-loss tunable bandpass filter using YIG/GGG film structures. *IEEE Microw Wirel Technol Lett*. 2023;33(3):259-262.
12. Faraday Dynamics. *Data sheet–IPD. UltraEM V2022*. Faraday Dynamics, Inc.; 2022.
13. Zhang J, Xu J-X, Yao C, Zhang XY. Miniaturized high-selectivity high-resistivity-silicon IPD bandpass filter based on multiple transmission paths. *IEEE Electron Device Lett*. 2024;45(4):534-537.

How to cite this article: Zhang Q, Cao Y, Wang G. Miniaturized IPD band pass filter with low insertion loss based on modified T-section for 5G applications. *Int J Numer Model*. 2024;37(3):e3248. doi:10.1002/jnm.3248